Pharmacy Education (2023) 23(2) 253 - 259
https://doi.org/10.46542/pe.2023.232.253259

IAI SPECIAL EDITION

RESEARCH ARTICLE

In silico study of aminothiazole, benzohydrazide, namoline, piridine, and parnate derivatives as Jumonji domain histone lysine demethylase (KDM1A, KDM4A, KDM4C, KDM4E, AND KDM5B) inhibitors in prostate cancer

Fauzan Zein Muttaqin[1], Revi Fahlevi[1], Hubbi Nasrullah Muhammad[2]

[1] Faculty of Pharmacy, Bhakti Kencana University, Bandung, Indonesia
[2] School of Pharmacy, Bandung Institute of Technology, Bandung, Indonesia

Keywords
Histone lysine demethylase
Molecular docking
Molecular dynamic

Correspondence
Fauzan Zein Muttaqin
Faculty of Pharmacy
Bhakti Kencana University
Bandung
Indonesia
fauzanzein@bku.ac.id

Abstract

Background: Prostate cancer is the second most common type of cancer in men. The histone lysine demethylase enzyme is believed to be one of the genetic factors that cause prostate cancer. Based on in vivo testing, a group of compounds from the aminothiazole, benzohydrazide, pyridine, namoline, and parnate classes have been experimentally proven to be inhibitors of the histone lysine demethylase enzyme. **Objective:** This study aimed to investigate the interaction of 20 compounds consisting of aminothiazole, benzohydrazide, pyridine, namoline, and parnate derivatives with histone lysine demethylase enzymes (KDM1A, KDM4A, KDM4C, KDM4E, and KDM5B) *in silico*. **Method:** Molecular docking was performed using Autodock Tools v.4.2.3 to obtain the affinity of test compounds against the target molecule. This was followed by molecular dynamics (MD) simulation of some test compounds with the lowest inhibition constant using Gromacs software. Toxicity prediction was conducted to predict the safety of the test compounds. **Result:** The docking results revealed the top five compounds for each receptor with the lowest inhibition constant and free binding energy value (ΔG), suggesting the best affinity to histone lysine demethylase enzymes. The results from MD showed that the compounds with the codes aminothiazole, pyridine, parnate 1, parnate 2, and parnate 5 were stable when bound to the KDM1A receptor. The toxicity test results also indicated that the test compounds were safe and had a low health risk, as they were neither genotoxic nor non-genotoxic carcinogens. **Conclusion:** Based on the research results, it can be concluded that compounds with the codes aminothiazole, pyridine, parnate 1, parnate 2, and parnate 5 can serve as inhibitors of histone lysine demethylase enzymes on the KDM1A receptor and are stable when bound to the receptor.

Introduction

Prostate cancer is a significant health concern for men worldwide. According to the World Health Organization (WHO), prostate cancer is the second most common cancer among men globally, with an estimated 1.4 million new cases and 375,000 deaths in 2020 (World Health Organization, 2023).

Prostate cancer is a type of cancer that develops in the prostate gland, a small gland located below the bladder in men. It is the most commonly diagnosed cancer in men and the second leading cause of cancer deaths in men in the United States (Jemal *et al*., 2017). The incidence of prostate cancer varies widely across different regions of the world, with the highest incidence rates observed in North America, Europe, and Australia. The lowest incidence rates are seen in

Asia, Africa, and South America. However, the incidence rates of prostate cancer in these regions have been increasing over the years, partly due to increased life expectancy and changes in lifestyle factors (Center *et al*., 2012).

The exact causes of prostate cancer are not fully understood, but it is believed to be related to a combination of genetic, environmental, and lifestyle factors (Heidenreich *et al*., 2014). Some known risk factors for prostate cancer include age, family history, and race (Siegel *et al*., 2021).

One of the challenges of prostate cancer is that it often does not cause symptoms in its early stages. As cancer grows, it can cause symptoms such as difficulty urinating, weak or interrupted urine flow, blood in the urine or semen, and pain or discomfort in the pelvic area. However, these symptoms can also be caused by other conditions, so it is important to see a doctor if they occur. Prostate cancer treatment depends on various factors, including the stage of cancer, the age and overall health of the patient, and the patient's preferences. Treatment options may include surgery to remove the prostate gland, radiation therapy, hormone therapy, or a combination of these treatments (American Cancer Society, 2022).

Histone lysine demethylase enzyme is estimated as one of the genetic factors causing prostate cancer. This enzyme causes methyl groups to detach from histones, resulting in the impact of histone methylation affecting the transcriptional activity of DNA. The process of effector protein binding to modified chromatin templates can lead to misrepresentation or activation of cancer cells. Thus, blocking histone lysine demethylase is one of the epigenetic mechanisms inhibiting growth and preventing cancer development, especially prostate cancer (Wang *et al.*, 2014).

Histone lysine demethylase enzymes (KDMs) are a group of epigenetic regulators that play a crucial role in regulating gene expression by removing methyl groups from histone lysine residues. The dysregulation of KDMs has been implicated in various diseases, including cancer. In particular, the overexpression of KDMs has been observed in several types of cancer, including prostate cancer, and is associated with poor patient prognosis (Jerónimo *et al.,* 2011). KDMs are classified into two main families: the Jumonji C (JmjC) domain-containing enzymes and the lysine-specific demethylase (LSD) enzymes. The JmjC domain-containing enzymes are involved in the demethylation of lysine residues in histones H3 and H4, whereas the LSD enzymes are responsible for the demethylation of lysine residues in histone H3 (Cloos *et al.,* 2008). Several small-molecule inhibitors have been developed to target KDMs to inhibit their activity and reduce cancer cell proliferation (Muttaqin *et al*., 2017).

In this research, we utilised computational simulations to investigate the interactions between compounds derived from coumarin, N-oxalylglycine, organo-selenium, organosulfur, and pyridine with KDM enzymes using molecular docking, molecular dynamics (MD), and toxicity prediction analyses. The findings of this study could potentially aid in the discovery and development of novel anticancer agents derived from natural sources.

Methods

Macromolecule preparation

Crystal structures of five KDM enzymes were downloaded from the website www.rcsb.org with PDB IDs 4UV8 (KDM1A), 3PDQ (KDM4A), 5FJK (KDM4C), 2W2I (KDM4E), and 5A3P (KDM5B) (Chang *et al*., 2011; Hillringhaus *et al*., 2011; Johansson *et al*., 2016; Vianello *et al*., 2014).

Ligand preparation

The chemical structures of twenty compounds of aminothiazole, benzohydrazide, namoline, piridine, and parnate derivatives in Table I were built using ChemOffice 2010 software, then optimised using Gaussian 09 software with Density Functional Theory (DFT) method, B3LYP, and basis set 6-31G (Frisch *et al*., 2009).

Molecular docking

Each ligand molecule was prepared for docking using AutoDock Tools 4.2.3. Hydrogen atoms were added, and partial charges of each atom resulting from the DFT calculations were incorporated. Grid maps were created by centering the grid box at the position of the natural ligand of each macromolecule with a spacing of 0.375 Å and size covering the binding cavity of each target. Each simulation used the Lamarckian genetic algorithm and 50 docking runs (Morris *et al*., 2009; Muttaqin *et al*., 2022).

Molecular dynamic simulation

Five ligands with the best docking score for each target based on free binding energy and inhibition constant were chosen for further MD study. The MD simulation was carried out using Gromacs 5.1.1 software (*GROMACS Documentation Release 2023 GROMACS Development Team*, 2023). The Amber99sb-ildn force field and the general AMBER force field (GAFF) were used to parameterise the atoms of the macromolecules and ligands, respectively.

Table I: The 20 aminothiazole, benzohydrazide, namoline, piridine, and parnate derivatives used

No	Compound	Code
1	N-(4-(4-(2-aminocyclopropyl)phenoxy)-1-(benzylamino)-1-oxobutan-2-yl)benzamide	PARNATE 1
2	N-(4-(3-(2-aminocyclopropyl)phenoxy)-1-(benzylamino)-1-oxobutan-2-yl)benzamide	PARNATE 2
3	N-(4-(2-aminocyclopropyl)phenyl)benzamide	PARNATE 3
4	benzyl 4-(2-aminocyclopropyl)phenylcarbamate	PARNATE 4
5	benzyl 1-(4-(2-aminocyclopropyl)phenylamino)-1-oxo-3-phenylpropan-2-ylcarbamate	PARNATE 5
6	benzyl 1-(4-(2-aminocyclopropyl)phenylamino)-3-(1H-indol-2-yl)-1-oxopropan-2-ylcarbamate	PARNATE 6
7	2-(perfluorophenyl)cyclopropanamine	PARNATE 7
8	2-(2-(benzyloxy)-3-fluorophenyl)cyclopropanamine	PARNATE 8
9	2-(2-(benzyloxy)-3,5-difluorophenyl)cyclopropanamine	PARNATE 9
10	2-(2-(3-(aminomethyl)benzyloxy)-3,5-difluorophenyl)cyclopropanamine	PARNATE 10
11	2-(2-(3-ethylbenzyloxy)-3,5-difluorophenyl)cyclopropanamine	PARNATE 11
12	N-(3-(2,4-dichlorophenoxy)propyl)-N-methylprop-2-yn-1-amine	PARNATE 12
13	3-[4-[(1R,2S)-2-aminocyclopropyl]phenyl]phenol	PARNATE 14
14	(S)-2-(4-(3-fluorobenzyloxy)benzylamino)propanamide	PARNATE 15
15	(R)-4-(4-isocyanophenyl)-5-(pyrrolidin-3-ylmethoxy)-2-p-tolylpyridine	PYRIDINE
16	N-(4-acetylthiazol-2-yl)-[1,1'-biphenyl]-3-sulfonamide	AMINOTHIAZOLE 1
17	N-(3-chlorophenyl)-5-(prop-1-en-2-yl)thiazol-2-amine	AMINOTHIAZOLE 2
18	N-(4-chlorophenyl)-5-(prop-1-en-2-yl)thiazol-2-amine	AMINOTHIAZOLE 3
19	3-chloro-6-nitro-2-(trifluoromethyl)-4aH-chromen-4(8aH)-one	NAMOLINE
20	(E)-N'-(1-(5-chloro-2-hydroxyphenyl)ethylidene)-3-(morpholinosulfonyl)Benzohidrazid	BENZOHYDRAZIDE

Energy minimisation was carried out on the macromolecules in vacuum pressure using the steepest descent algorithm, followed by solvating the macromolecule with TIP3P water molecules in an octahedron box. Positive and negative ions were added to the system at a concentration of 0.15 N to neutralise all charges. Energy minimisation was again performed on the macromolecule/solvent/ion system to release strains resulting from the solvation procedure; the steepest descent algorithm was used again.

Next, the system was carefully heated to 310 K and pressurized to 1 atm using the constant-volume, constant-temperature (NVT) and constant-pressure, constant-temperature (NPT) ensembles. The Berendsen thermostat coupling was used to maintain the system temperature and pressure. The Particle Mesh Ewald (PME) method with a cut-off value of 5.0 Å was used to compute long-range interactions. The system's stability was evaluated by analysing the root mean square deviation (RMSD) and root mean square fluctuation (RMSF) of the protein backbones. A production simulation run was carried out on each macromolecule for two nanoseconds (ns). Analysis of the stability of ligand-protein interactions was performed by calculating the RMSD and RMSF values of the atoms at the protein binding sites throughout the simulation.

Toxicity prediction

Toxicity prediction was performed using Toxtree 2.6.6. Three methods were used for the prediction: Cramer rules, Kroes TTC decision tree, and Benigni/Bossa rulebase (Patlewicz *et al*., 2008).

Results

The docking results of the best five compounds for each target can be seen in Tables II-VI.

Table II: The docking results of the best five compounds against Histone Lysine Demethylase 1A (KDM1A)

Code	Free binding energy (kcal/mol)	Inhibition constant
Parnate 1	-9.76	69.72 nM
Parnate 2	-7.92	1.58 µM
Parnate 5	-8.34	768.51 nM
Pyridine	-9.15	195.97 nM
Aminothiazole 1	-7.37	3.94 µM

Table III: The docking results of the best five compounds against Histone Lysine Demethylase 4A (KDM4A)

Code	Free binding energy (kcal/mol)	Inhibition constant
Parnate 1	-6.9	8.79 µM
Pyridine	-8.04	1.29 µM
Namoline	-7.16	5.64 µM
Benzohydrazide	-7.03	7.06 µM
Parnate 14	-6.74	11.55 µM

Table IV: The docking results of the best five compounds against Histone Lysine Demethylase 4C (KDM4C)

Code	Free binding energy (kcal/mol)	Inhibition constant
Parnate 3	-6.52	16.58 µM
Parnate 11	-6.51	16.57 µM
Pyridine	-7.15	5.73 µM
Parnate 8	-6.37	21.45 µM
Parnate 14	-6.52	16.74 µM

Table V: The docking results of the best five compounds against Histone Lysine Demethylase 4E (KDM4E)

Code	Free binding energy (kcal/mol)	Inhibition constant
Parnate 9	-6.55	15.86 µM
Parnate 10	-6.07	35.83 µM
Parnate 11	-6.8	10.36 µM
Namoline	-6.67	12.98 µM
Parnate 14	-6.1	33.98 µM

Table VI: The docking results of the best five compounds against Histone Lysine Demethylase 5B (KDM5B)

Code	Free binding energy (kcal/mol)	Inhibition constant
Parnate 11	-7.07	6.57 µM
Pyridine	-8.24	912.30 nM
Benzohydrazide	-6.73	11.75 µM
Parnate 13	-6.75	11.24 µM
Parnate 14	-6.71	12.12 µM

The RMSD and RMSF curves of the best five ligands for each target can be seen in Figures 1-5.

The toxicity prediction of 20 compounds of aminothiazole, benzohydrazide, namoline, pyridine, and parnate derivatives can be seen in Table VII.

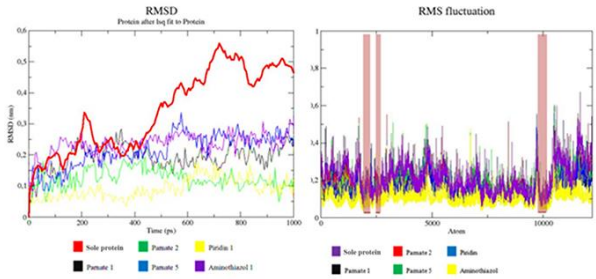

Figure 1: RMSD and RMSF curves of the KDM1A sole protein and in complex with ligand parnate 1, parnate 2, parnate 5, pyridine, and aminothiazole 1

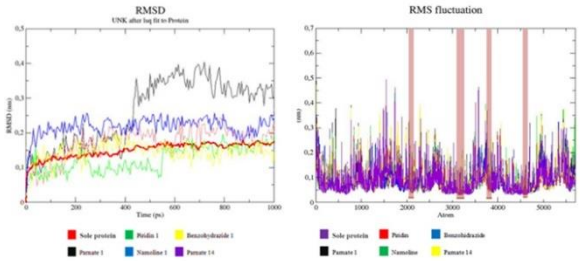

Figure 2: RMSD and RMSF curves of the KDM4A sole protein and in complex with ligand parnate 1, pyridine, namoline, benzohydrazide, and parnate 14

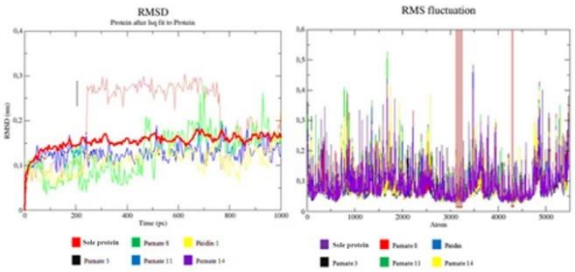

Figure 3: RMSD and RMSF curves of the KDM4C sole protein and in complex with ligand parnate 3, parnate 11, pyridine, parnate 8, and parnate 14

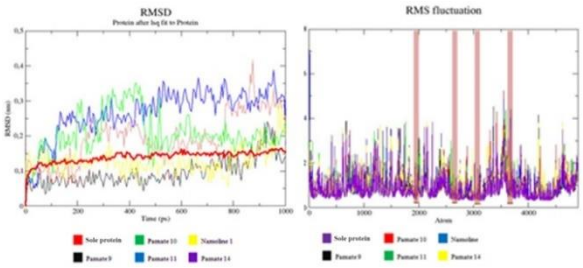

Figure 4: RMSD and RMSF curves of the KDM4E sole protein and in complex with ligand parnate 9, parnate 10, parnate 11, namoline, and parnate 14

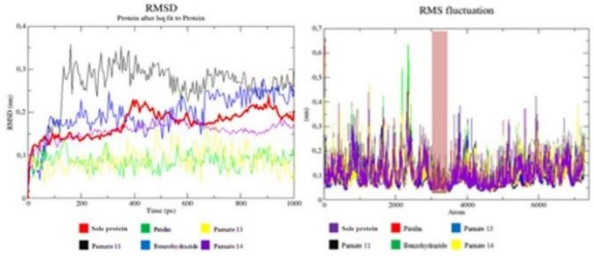

Figure 5: RMSD and RMSF curves of the KDM5B sole protein and in complex with ligand parnate 11, pyridine, benzohydrazide, parnate 13, and parnate 14

Table VII: The toxicity prediction of 20 aminothiazole, benzohydrazide, namoline, pyridine, and parnate derivatives

Code	Toxicity		Benigni / Bossa
	Cramer rules	Kroes TTC	
PARNATE 1	High (Class III)	No	Negative
PARNATE 2	High (Class III)	No	Negative
PARNATE 3	High (Class III)	No	Negative
PARNATE 4	High (Class III)	No	Negative
PARNATE 5	High (Class III)	No	Negative
PARNATE 6	High (Class III)	No	Negative
PARNATE 7	High (Class III)	No	Negative
PARNATE 8	High (Class III)	No	Negative
PARNATE 9	High (Class III)	No	Negative
PARNATE 10	High (Class III)	No	Negative
PARNATE 11	High (Class III)	No	Negative
PARNATE 12	High (Class III)	No	Negative
PYRIDINE	High (Class III)	No	Negative
AMINOTIAZOL	High (Class III)	No	Negative
NAMOLINE	High (Class III)	No	Negative
BENZOHYDRAZIDE	High (Class III)	No	Negative
AMINOTHIAZOLE 1	High (Class III)	No	Negative
AMINOTHIAZOLE 2	High (Class III)	No	Negative
PARNATE 13	High (Class III)	No	Negative
PARNATE 14	High (Class III)	No	Negative

Discussion

From the docking results of the test compounds against each target, the top five best test compounds were obtained for each target based on the Free Energy of Binding (ΔG) and inhibition constant. The lower the ΔG value, the more stable the ligand-receptor binding will be and the greater the ability of a ligand to interact with the enzyme.

Based on the docking of test compounds with Histone Lysine Demethylase 1A (KDM1A), the top five compounds were obtained; namely compounds with codes parnate 1, parnate 2, parnate 5, pyridine, and aminothiazole 1 as shown in Table II. The compound N-(4-(4-(2-aminocyclopropyl)phenoxy)-1-(benzylamino)-1-oxobutan-2-yl)benzamide (code Parnate 1) had the most negative ΔG, indicating the best interaction. The data in Table III showed that compounds with codes parnate 1, pyridine, namoline, benzohydrazide, and parnate 14 were the top five compounds against KDM4A, with (R)-4-(4-isocyanophenyl)-5-(pyrrolidin-3-ylmethoxy)-2-p-tolylpyridine (code Pyridine) having the best interaction. Table IV showed that compounds with codes parnate 3, parnate 11, pyridine, parnate 8, and parnate 14 were the top five compounds against KDM4C, with (R)-4-(4-isocyanophenyl)-5-(pyrrolidin-3-ylmethoxy)-2-p-tolylpyridine (code Pyridine) having the best interaction. Table V showed that compounds with codes parnate 9, parnate 10, parnate 11, namoline, and parnate 14 were the top five compounds against KDM4E, with 2-(2-(benzyloxy)-3-fluorophenyl)cyclopropanamine (code Parnate 8) having the best interaction. Moreover, Table VI showed that compounds with codes parnate 11, pyridine, benzohydrazide, parnate 13, and parnate 14 were the top five compounds against KDM5B, (R)-4-(4-isocyanophenyl)-5-(pyrrolidin-3-ylmethoxy)-2-p-tolylpyridine (code Pyridine) having the best interaction.

The docking results of all test compounds to each target have negative free binding energy. This indicates that the binding between ligand and receptor occurs spontaneously.

The MD simulation results obtained the Root Mean Square Deviation (RMSD) and Root Mean Square Fluctuation (RMSF) curves of each of the top five compounds against each target, as shown in Figures 1-5. The RMSD curve in Figures 1-5 showed that the test compounds with the most stable binding to their receptors are found on the KDM1A receptor. All of the five ligands were able to stabilise the protein in general, marked by lower RMSD values compared to the lone protein. While for the other KDM receptors, there were still test compounds with higher RMSD values than the lone protein.

RMSD is a common metric used in MD simulations to evaluate the stability and similarity of protein structures over time. It is a measure of the average distance between the atoms of two protein structures, which are typically compared to each other over a time frame. During an MD simulation, the protein structure fluctuates and changes shape due to thermal motions and interactions with the solvent molecules. To quantify these changes, the MD trajectory is compared to an initial or reference structure, typically the crystal structure or the minimized starting structure. The RMSD is calculated as the square root of the average of the squared distances between the atoms of the two structures. A low RMSD value indicates that the protein structure is stable and has not undergone significant conformational changes during the simulation. A high RMSD value indicates that the protein structure has undergone significant structural changes, such as unfolding or large-scale rearrangements.

From the RMSF curve in Figures 1-5, it could be observed that all amino acid residues in each receptor that interact with ligands were predicted to be stable due to the low fluctuation.

RMSF is a measure of the deviation of atomic positions from their average position over the course of a MD simulation. RMSF is calculated for each residue that makes up the protein by observing the extent of the fluctuation of each residue's movement during the simulation. The RMSF value describes the conformational shift of each amino acid residue that gives protein flexibility. It is often used to assess the flexibility and mobility of different parts of a protein or other biomolecule. During a MD simulation, atoms move around due to thermal fluctuations, causing the molecule to undergo conformational changes. RMSF can be calculated by measuring the deviation of each atom's position from the average position over the course of the simulation. RMSF values are typically plotted as a function of residue number, allowing researchers to identify regions of the molecule that are particularly flexible or rigid. High RMSF values indicate more mobile regions, while low RMSF values indicate more stable regions. RMSF analysis can be particularly useful in identifying binding sites or regions that undergo conformational changes upon binding to a ligand or other molecule.

The toxicity prediction aims to determine the potential of a compound as a poison that can cause adverse effects on the body's systems. The toxicity prediction results can be obtained using the ToxTree software. Three parameters are used: Cramer Rules, Kroes TTC decision tree, and Benigni Bossa Rulebase.

Based on the toxicity prediction results using the Cramer Rules of 20 test compounds, all tested compounds fall into class III (High). This means that these compounds have the highest level of toxicity based on the parameters in the Cramer Rules. The presence of aromatic groups in the test compounds caused all of them to be included in the III (High Class) (Cramer *et al*., 1978).

The Kroes TTC decision tree aims to determine the risk of exposure to the test compounds (Kroes *et al*., 2004). Based on the toxicity prediction results using Kroes TTC decision tree for the 20 test compounds, all tested compounds are estimated not to threaten health.

The Benigni Bossa Rulebase is used to determine the risk of mutagenesis and carcinogenesis of the test compounds (Benigni *et al*., 2007). Based on the toxicity prediction results with the Benigni Bossa Rulebase of the 20 test compounds, all test compounds are not at risk of causing carcinogenesis, both genotoxic carcinogens and non-genotoxic carcinogens.

Conclusion

Based on the research results, it can be concluded that compounds with the codes aminothiazole, pyridine, parnate 1, parnate 2, and parnate 5 can serve as inhibitors of histone lysine demethylase enzymes on the KDM1A receptor and are stable when bound to the receptor.

References

American Cancer Society. (2022). *Prostate Cancer*. https://www.cancer.org/cancer/prostate-cancer.html

Benigni, R., Bossa, C., Netzeva, T., Rodomonte, A., & Tsakovska, I. (2007). Mechanistic QSAR of aromatic amines: New models for discriminating between homocyclic mutagens and nonmutagens, and validation of models for carcinogens. *Environmental and Molecular Mutagenesis*, **48**(9), 754–771. https://doi.org/10.1002/em.20355

Center, M. M., Jemal, A., Lortet-Tieulent, J., Ward, E., Ferlay, J., Brawley, O., & Bray, F. (2012). International variation in prostate cancer incidence and mortality rates. In *European Urology,* **61**(6), 1079–1092. https://doi.org/10.1016/j.eururo.2012.02.054

Chang, K. H., King, O. N. F., Tumber, A., Woon, E. C. Y., Heightman, T. D., Mcdonough, M. A., Schofield, C. J., & Rose, N. R. (2011). Inhibition of histone demethylases by 4-Carboxy-2,2'-Bipyridyl compounds. *ChemMedChem*, **6**(5), 759–764. https://doi.org/10.1002/cmdc.201100026

Cloos, P. A. C., Christensen, J., Agger, K., & Helin, K. (2008). Erasing the methyl mark: Histone demethylases at the center of cellular differentiation and disease. In *Genes and Development*, **22**(9), 1115–1140. https://doi.org/10.1101/gad.1652908

Cramer, G. M., Ford, R. A., & Hall, R. L. (1978). *Review Section ESTIMATION OF TOXIC HAZARD-A DECISION TREE APPROACH*, **16**. Pergamon Press. https://doi.org/10.1016/S0015-6264(76)80522-6

Frisch, M. J., Trucks, G. W., Schlegel, H. B., Scuseria, G. E., Robb, M. A., Cheeseman, J. R., Scalmani, G., Barone, V., Mennucci, B., Petersson, G. A., Nakatsuji, H., Caricato, M., Li, X., Hratchian, H. P., Izmaylov, A. F., Bloino, J., Zheng, G., Sonnenberg, J. L., Hada, M., … Fox, D. J. (2009). *Gaussian 09, Revision E.01*. Gaussian, Inc

GROMACS Documentation Release 2023 GROMACS development team. (2023)

Heidenreich, A., Bastian, P. J., Bellmunt, J., Bolla, M., Joniau, S., Van Der Kwast, T., Mason, M., Matveev, V., Wiegel, T., Zattoni, F., & Mottet, N. (2014). EAU guidelines on prostate cancer. Part 1: Screening, diagnosis, and local treatment with curative intent - Update 2013. *European Urology*, **65**(1), 124–137. https://doi.org/10.1016/j.eururo.2013.09.046

Hillringhaus, L., Yue, W. W., Rose, N. R., Ng, S. S., Gileadi, C., Loenarz, C., Bello, S. H., Bray, J. E., Schofield, C. J., & Oppermann, U. (2011). Structural and evolutionary basis for the dual substrate selectivity of human KDM4 histone demethylase family. *Journal of Biological Chemistry*, **286**(48), 41616–41625. https://doi.org/10.1074/jbc.M111.283689

Jemal, A., Ward, E. M., Johnson, C. J., Cronin, K. A., Ma, J., Ryerson, A. B., Mariotto, A., Lake, A. J., Wilson, R., Sherman, R. L., Anderson, R. N., Henley, S. J., Kohler, B. A., Penberthy, L., Feuer, E. J., & Weir, H. K. (2017). Annual Report to the Nation on the Status of Cancer, 1975-2014, Featuring Survival. In *Journal of the National Cancer Institute*, **109**(9). Oxford University Press. https://doi.org/10.1093/jnci/djx030

Jerónimo, C., Bastian, P. J., Bjartell, A., Carbone, G. M., Catto, J. W. F., Clark, S. J., Henrique, R., Nelson, W. G., & Shariat, S. F. (2011). Epigenetics in prostate cancer: Biologic and clinical relevance. In *European Urology*, **60**(4), 753–766). https://doi.org/10.1016/j.eururo.2011.06.035

Johansson, C., Velupillai, S., Tumber, A., Szykowska, A., Hookway, E. S., Nowak, R. P., Strain-Damerell, C., Gileadi, C., Philpott, M., Burgess-Brown, N., Wu, N., Kopec, J., Nuzzi, A., Steuber, H., Egner, U., Badock, V., Munro, S., Lathangue, N. B., Westaway, S., … Oppermann, U. (2016). Structural analysis of human KDM5B guides histone demethylase inhibitor development. *Nature Chemical Biology*, **12**(7), 539–545. https://doi.org/10.1038/nchembio.2087

Kroes, R., Renwick, A. G., Cheeseman, M., Kleiner, J., Mangelsdorf, I., Piersma, A., Schilter, B., Schlatter, J., Van Schothorst, F., Vos, J. G., & Würtzen, G. (2004). Structure-based thresholds of toxicological concern (TTC): Guidance for application to substances present at low levels in the diet. *Food and Chemical Toxicology*, **42**(1), 65–83. https://doi.org/10.1016/j.fct.2003.08.006

Morris, G. M., Ruth, H., Lindstrom, W., Sanner, M. F., Belew, R. K., Goodsell, D. S., & Olson, A. J. (2009). Software news and updates AutoDock4 and AutoDockTools4: Automated docking with selective receptor flexibility. *Journal of Computational Chemistry*, **30**(16), 2785–2791. https://doi.org/10.1002/jcc.21256

Muttaqin, F. Z., Fakih, T. M., & Muhammad, H. N. (2017). Molecular docking, molecular dynamics, and in silico toxicity prediction studies of coumarin, N-Oxalylglycine, organoselenium, organosulfur, and pyridine derivatives as histone lysine demethylase inhibitors. *Asian Journal of Pharmaceutical and Clinical Research*, **10**(12). https://doi.org/10.22159/ajpcr.2017.v10i12.19348

Muttaqin, F. Z., Sari, A. P. R., & Kurniawan, F. (2022). Molecular docking study of vemurafenib derivatives on melanoma inhibitory activity (MIA) as anti-melanoma. *Pharmacy Education*, **22**(2), 284–288. https://doi.org/10.46542/pe.2022.222.284288

Patlewicz, G., Jeliazkova, N., Safford, R. J., Worth, A. P., & Aleksiev, B. (2008). An evaluation of the implementation of the Cramer classification scheme in the Toxtree software. *SAR and QSAR in Environmental Research*, **19**(5–6), 495–524. https://doi.org/10.1080/10629360802083871

Siegel, R. L., Miller, K. D., Fuchs, H. E., & Jemal, A. (2021). Cancer Statistics, 2021. *CA: A Cancer Journal for Clinicians*, **71**(1), 7–33. https://doi.org/10.3322/caac.21654

Vianello, P., Botrugno, O. A., Cappa, A., Ciossani, G., Dessanti, P., Mai, A., Mattevi, A., Meroni, G., Minucci, S., Thaler, F., Tortorici, M., Trifiró, P., Valente, S., Villa, M., Varasi, M., & Mercurio, C. (2014). Synthesis, biological activity and mechanistic insights of 1-substituted cyclopropylamine derivatives: A novel class of irreversible inhibitors of histone demethylase KDM1A. *European Journal of Medicinal Chemistry*, **86**, 352–363. https://doi.org/10.1016/j.ejmech.2014.08.068

Wang, L.-Y., Guo, W., Kim, K., Pochampalli, M., Hung, C.-L., Izumiya, Y., & Kung, H.-J. (2014). Histone Demethylases in Prostate Cancer. In R. Kumar (Ed.), *Nuclear Signaling Pathways and Targeting Transcription in Cancer. Cancer Drug Discovery and Development*. Humana Press. https://doi.org/https://doi.org/10.1007/978-1-4614-8039-6_15

World Health Organization. (2023). *Prostate cancer*. https://www.who.int/cancer/prevention/diagnosis-screening/prostate-cancer/en/